Assessment of effective-medium theories in the analysis of nucleation and microscopic surface roughness evolution for semiconductor thin films

H. Fujiwara,* Joohyun Koh, P. I. Rovira, and R. W. Collins
Materials Research Laboratory, Center for Thin Film Devices, and Department of Physics, Pennsylvania State University, University Park, Pennsylvania 16802
(Received 30 September 1999)

Real-time spectroscopic ellipsometry (SE) data collected during the nucleation and growth of hydrogenated amorphous silicon (*a*-Si:H) thin films have been analyzed by applying one and two layer optical models incorporating different effective medium theories (EMT's). The purpose of the EMT's is to simulate the dielectric functions of the microscopically inhomogeneous nucleating and surface roughness layers used in the models. Five one-parameter EMT's have been considered in this study for the characterization of three classes of microscopically inhomogeneous layers, including (i) 5–20 Å-thick nucleating layers consisting of isolated *a*-Si:H clusters on the underlying substrate, (ii) 10–15 Å-thick nucleation-induced surface roughness layers on very thin (<200 Å) *a*-Si:H films, and (iii) 40–80 Å-thick substrate-induced surface roughness layers on thicker (>2500 Å) a-Si:H films. In all three applications, the Bruggeman effective medium approximation (EMA) provides the best overall fits to the time evolution of the SE data, and complexities beyond the simple one-parameter EMA cannot be justified in view of existing experimental limitations. Furthermore, many of the general features of nucleation, coalescence, and bulk layer growth deduced in the SE analysis and used in previous studies to understand and optimize materials and device fabrication, are found to be essentially independent of the EMT used in the analysis.

I. INTRODUCTION

Numerous approaches have been developed over the years to predict the effects of rough surfaces and interfaces on incident light waves.[1] These approaches include, for example, (i) diffraction theories,[2,3] (ii) classical scattering theories and perturbation theories applying expansions of Maxwell's equations about a mean smooth surface,[4,5] (iii) first-principles theories of the electromagnetic response of systems having spatial fluctuations,[6] and (iv) effective medium theories (EMT's) with surface layer optical models.[7,8] Approach (iv) has been widely employed when the dimensions of the inhomogeneities and all correlation lengths associated with the roughness are smaller than the wavelength of the light, i.e., when the roughness is ''microscopic.''[9] In this case, the effect of the surface roughness on the polarization of the reflected light measured in the far field can be simulated by interposing one or more layers between a perfect substrate and the ambient.[7,10] This simple approach is ideally suited for surface characterization using optical methods such as reflectometry and ellipsometry since their analysis procedures are based on models of light reflection from one or more plane-parallel interfaces, as described by the Fresnel equations.[11,12] Ellipsometric studies over the decade starting from the late 1960s adopted such an approach for the analysis of microscopic surface roughness, often in conjunction with the Lorentz-Lorenz EMT to calculate the effective optical properties of the roughness ''layer'' [see, e.g., Eq. (1) of Ref. 13]. Because such ellipsometric studies utilized one or a few selected wavelengths, it was generally not possible to assess the validity of the EMT or the relative effectiveness of different EMT formulations.

With the development of highly accurate instruments for spectroscopic ellipsometry (SE) starting in the mid-1970s,[14] it became possible to assess the validity of the surface roughness layer optical model and to identify the EMT's that yield the best fits in the analysis of SE data over a wide spectral range. The first such study was performed on rough amorphous silicon (*a*-Si) thin films in 1979 by Aspnes, Theeten, and Hottier.[15] In the study of Ref. 15, which compared three one-parameter EMT's, the Bruggeman and the Maxwell-Garnett EMT formulations were found to represent the SE data adequately whereas the Lorentz-Lorenz theory yielded much poorer results. Among all three EMT's, that of Bruggeman provided the best overall fit to the SE data. The study of Ref. 15 on *a*-Si films and a similar one on gold films,[16] entrenched the surface roughness layer optical model along with the Bruggeman effective medium approximation as the accepted method for the analysis of SE data for bulk materials and thin films having microscopically rough surfaces or interfaces.[17]

The motivations of such surface characterization by SE have been twofold: (i) to measure the roughness in order to eliminate its effects and extract the true dielectric function of the underlying material or thin film, and (ii) to deduce details on the roughness itself (e.g., thickness, effective dielectric function) and obtain insights into materials and thin film preparation.[17] With the availability of scanning probe microscopies such as atomic force microscopy (AFM), powerful tools are now available to support surface characterization by SE. As an example, the bearing ratio from a microscopic image analysis of a rough surface can be discretized into a number of surface layers of defined thicknesses whose optical properties are calculated from the EMT. With the surface structure fully quantified, the bulk material dielectric function can be deduced by numerical inversion of the SE data.[18] As a second example, parameters

0163-1829/2000/61(16)/10832(13)/$15.00 PRB 61 ©2000 The American Physical Society

from AFM image analyses can be correlated with the results of SE data analyses to ensure that sample-to-sample variations in surface roughness layer thickness deduced on the basis of the EMT are supported by direct observations.[19]

Optical models for nucleating thin films consisting of isolated, microscopic-scale clusters on the substrate surface have been developed along the same lines as those for microscopic roughness, but with more extensive history.[9] In the 1900s, Maxwell-Garnett derived the effective medium theory that bears his name, using it to explain the color observed in transmission through discontinuous, thin metallic films.[20,21] In this approach, the thin film is modeled as a regular array of spherical particles embedded within the ambient medium. Much later, in perhaps the most comprehensive ex situ study of nucleating thin films to date, Norrman *et al.* demonstrated that a generalized form of the Maxwell-Garnett theory using a distribution of ellipsoidal particles on the substrate surface best-fit transmittance spectra at normal incidence for discontinuous gold films.[22] The strength of this latter study resided in its use of scanning electron microscopy to eliminate all but one free microstructural parameter in the optical analysis. In contrast, Hottier and Theeten, relying on the SE study of Ref. 15, applied the Bruggeman effective medium approximation to deduce microstructural information from real-time ellipsometry data collected at one wavelength during the nucleation of *a*-Si thin films on dielectric surfaces.[23] Parameters such as the critical thickness at which nuclei make contact to form a continuous layer could be determined. With the recent widespread use of AFM, the validity of run-to-run variations in the nucleation parameters deduced in analyses of real-time ellipsometry data for thin films can be supported by direct microscopic studies of the films performed *ex situ* after terminating the deposition at different elapsed times.[24,25]

In spite of the increasing use of the Bruggeman effective medium approximation over the last two decades for the analysis of microscopic roughness and discontinuous nucleating films, further detailed assessments of EMT's similar to that of Ref. 15 have been lacking. The more recent development of real-time SE (Ref. 26) has provided an opportunity to reassess EMT's. Real-time SE has the advantage of being able to collect spectra during the full microstructural evolution of the film from the nucleation regime, when the film can be modeled as a single layer on the substrate, through to the opaque regime when the film can be modeled as a bulk material with a roughness layer on top. The results of such an analysis for polycrystalline aluminum film growth on SiO_2-covered silicon wafers led to the generalized Maxwell-Garnett theory for describing initial nucleation and to the Bruggeman effective medium approximation for describing the roughness layer evolution on the coalesced aluminum film.[27] In the case of aluminum, however, the best EMT's are more difficult to identify owing to the particle and grain size effects on the dielectric functions of the aluminum clusters and coalesced films, respectively.

As a result, we have been motivated to reconsider the EMT assessment in the case of *a*-Si:H nucleation, coalescence, and roughness evolution. For this material, any size effects on the optical properties are significantly weaker than for crystalline materials owing to the lack of long-range order.[28] In addition, analyses of real-time data sets consisting of several to a few hundred spectra in different sample states is expected to provide a more definitive assessment of the EMT's than the prior analyses of ex situ data from a few samples. In addition, although pioneering for its time, Ref. 15 contains deficiencies that further motivate such a reconsideration. First, the dielectric function $\varepsilon=\varepsilon_1+i\varepsilon_2$ of the *a*-Si reference film used by Aspnes *et al.* exhibited a peak value for ε_2 of ~21 near 3.5 eV in contrast to later studies of *a*-Si that showed a peak of ~29 near 3.75 eV.[29] Thus, the reference film was likely to exhibit considerable roughness itself. Second, the roughness layer on the *a*-Si used in the EMT assessment was ~230–270 Å, much thicker than most layers on the materials and films to which this approach is now being applied.[17] In the *ex situ* analysis of Ref. 15, it was necessary to use such a thick layer in order to avoid ambiguity that occurs when the native oxide layer thickness is a significant fraction of the roughness thickness. In the presence of this ambiguity, no statement at all can be made regarding the most appropriate EMT. The native oxide is avoided in real time measurements, and EMT assessments are possible for much thinner roughness layers.

II. EXPERIMENTAL PROCEDURES

A. Effective medium theories

In this study, we have applied three simple EMT's for isotropic composites along with two limiting EMT forms in assessing which one(s) may be preferred for the determination of the dielectric functions of nucleating and surface roughness layers. The three EMT's selected for assessment here, including the Bruggeman effective medium approximation, the Maxwell-Garnett theory, and the Lorentz-Lorenz theory, are those used most widely to model dielectric functions of microscopic composite materials in the optical frequency range.[7,8] Other EMT's for example those of Sen, Scala, and Cohen[30] and McLachlan[31] that have been applied successfully to model the dc and low-frequency conductance of composites, are not considered.

The general form that encompasses the five EMT formulations for the two-component composite of *a*-Si:H and void encountered here is given by

$$\varepsilon=\frac{\varepsilon_a\varepsilon_v+\kappa\varepsilon_h(f_a\varepsilon_a+f_v\varepsilon_v)}{\kappa\varepsilon_h+(f_a\varepsilon_v+f_v\varepsilon_a)}, \qquad (1)$$

where $\kappa=(1/q)-1$ and q $(0\leqslant q\leqslant 1)$ is the screening parameter.[7] ε is the dielectric function of the composite layer, which in this case is either a discontinuous layer of nuclei or a surface roughness layer. ε_h is the host dielectric function, ε_a and f_a are the dielectric function and volume fraction of the *a*-Si:H component, and ε_v and f_v are the dielectric function and volume fraction of the void component. The validity of the EMT rests on two key assumptions as described in detail in the literature.[7,8] First, the scale of the compositional variation must be much smaller than the minimum wavelength in the measurement, so that light scattering is negligible. Second, in order to apply Eq. (1) directly, the dielectric function of the components must be size and shape independent. This latter restriction can be avoided in some cases by using a size dependent dielectric response for ε_a explicitly in Eq. (1).[22,27]

The choice $\varepsilon_h = \varepsilon$ in Eq. (1) defines the Bruggeman effective medium approximation, denoted hereafter as the EMA. $\varepsilon_h = \varepsilon_a$ defines the Maxwell-Garnett (MG) theory with the host being the *a*-Si:H phase, and finally, $\varepsilon_h = \varepsilon_v = 1$ defines the Lorentz-Lorenz (LL) theory.[7] Setting $q = \frac{1}{3}$ so that $\kappa = 2$ in Eq. (1) is appropriate for spherical inclusions and leads to an isotropic dielectric function. Throughout this study, the isotropic forms of the EMA, MG, and LL formulations are applied with $\kappa = 2$. Setting $q = 0$ leads to a composite dielectric function that is a volume-fraction weighted average of the component material dielectric functions, i.e., $\varepsilon = f_a \varepsilon_a + f_v \varepsilon_v$. This corresponds to no screening that occurs when the optical electric fields are parallel to the phase boundaries. Setting $q = 1$ leads to a composite dielectric function given by $\varepsilon^{-1} = f_a \varepsilon_a{}^{-1} + f_v \varepsilon_v{}^{-1}$. This corresponds to maximum screening that occurs when the fields are normal to the phase boundaries. When $q \neq 1/3$, the microscopic structure is anisotropic, and this leads to anisotropy in the dielectric function.[22] For the two limiting cases of the dielectric function, we ignore anisotropic effects in the analysis of the data. Thus, we assume that the fields are either parallel or perpendicular to the phase boundaries, even though this situation would hardly be expected when the angle of incidence is neither normal nor grazing.

Generally, it is anticipated that using a vacuum host as in the LL theory would be inappropriate for composites having two solid state components that are space-filling.[15] The MG theory is anticipated to be appropriate for dilute composites in which a lower volume fraction material is embedded in a solid state host material, such as a low-volume fraction of voids in *a*-Si. The EMA is most likely to represent an aggregate microstructure in which neither component can be viewed as the host. The EMA, however, approaches the MG theory in the limit of a dilute composite. Figure 1 shows the composite dielectric functions of a 0.5/0.5 *a*-Si:H/void volume fraction mixture at the deposition temperature of 200 °C for the MG, EMA, and LL formulations with $q = \frac{1}{3}$, and for the two limiting forms corresponding to $q = 0$ and $q = 1$. In this figure, the $q = 1$ limit and the LL theory exhibit behavior similar to a dielectric material with $\varepsilon_2 \approx 0$ throughout the energy range covered. In fact, if the $q = 1$ limit or the LL were valid it would be virtually impossible to distinguish between thin surface roughness and native SiO_2 overlayers on *a*-Si surfaces. This situation exists because the dielectric function of SiO_2 and the effective dielectric functions of *a*-Si:H/void composites from the $q = 1$ limit and the LL are quite similar for selected f_a values of the composites. As a result, there is a strong motivation for performing the EMT assessments in situ and in real time since the presence of any SiO_2 overlayers can be ruled out in this case. In contrast to the LL and $q = 1$ limiting form in Fig. 1, the EMA, MG, and $q = 0$ limiting form show dielectric functions that are similar in overall shape to *a*-Si:H, but varying in magnitude.

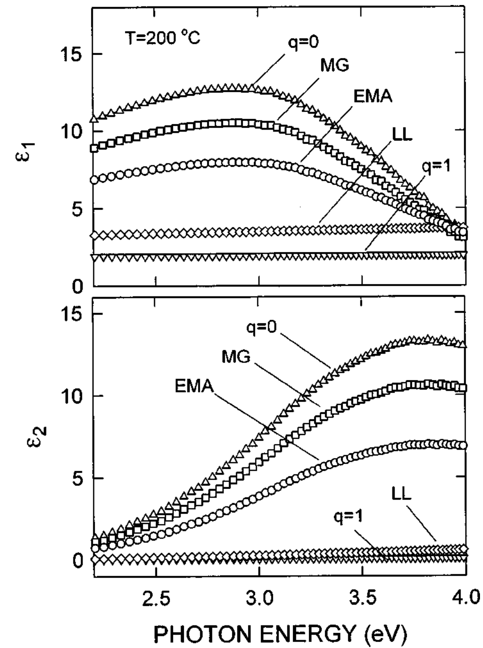

FIG. 1. Dielectric function spectra at the measurement temperature of 200 °C for microscopic mixtures consisting of 0.5/0.5 volume fractions of *a*-Si:H/void calculated using different EMT formulations ($q = 0$: zero-screening limit; $q = 1$: maximum screening limit; MG: Maxwell-Garnett EMT with *a*-Si:H as the host medium; EMA: Bruggeman effective medium approximation; LL: Lorentz-Lorenz EMT). The dielectric function for the *a*-Si:H component in the EMT was deduced from real-time SE measurements.

B. Thin-film deposition and characterization

The *a*-Si:H thin films studied here were prepared by plasma-enhanced chemical vapor deposition using pure SiH_4 gas at a substrate temperature of 200 °C. The rf power flux at the grounded substrate electrode was 70 mW/cm^2, the SiH_4 pressure was 0.07 Torr, and the SiH_4 flow was 5 stand. cm^3/min (sccm). Under these conditions, the deposition rate of the film is 1.3 Å/s. The relatively low flow of SiH_4 used here may lead to partial gas depletion in the discharge and short lifetime radicals such as SiH and SiH_2 that limit coalescence and generate a thicker roughness layer on the film surface.[32]

For studies of thick roughness layers (Sec. III A), *a*-Si:H was deposited on microcrystalline SnO_2:F and Si (μc-Si:H) substrate films, the latter films having root-mean square (rms) roughness values measured by AFM in the range of 100-200 Å. The SnO_2:F was prepared by chemical vapor deposition to a thickness of 440 Å, which led to a fine-grained structure. The μc-Si:H was prepared by plasma-enhanced chemical vapor deposition to a thickness of 6000 Å. For both substrates, the overdeposited *a*-Si:H films exhibited 40-80 Å-thick roughness layers induced by the roughness on the substrates. These *a*-Si:H films were studied after having reached opacity at the minimum photon energy of analysis (2.48 eV). For studies of the thin roughness layers that evolve during nuclei coalescence and bulk film growth (Sec. III B), the *a*-Si:H was deposited on a crystalline Si (*c*-Si) wafer with its native oxide intact. For studies of nucleating *a*-Si:H (Sec. III C), opaque Cr was used as the substrate in order to achieve higher sensitivity to the dielectric function of the ultrathin film. The Cr was prepared by low-pressure magnetron sputtering on a *c*-Si wafer in an attempt to minimize roughness, which would then be imposed on the overdeposited *a*-Si:H film. A comparison of the real time SE analyses of the 200 Å *a*-Si:H depositions on *c*-Si and Cr yielded the same value for the final roughness layer thickness (13 Å, using the EMA). As a result, we conclude that the

roughness is controlled by the nucleation and coalescence processes in both cases and is not influenced by substrate roughness.

In the studies of Secs. III B and III C, SE data were collected from the substrates immediately before plasma ignition for *a*-Si:H deposition. These spectra provided the dielectric function of the bulk substrate material at the deposition temperature of 200 °C, as well as the characteristics of any overlayers on the substrate surface. This information was needed for subsequent analysis of the real-time SE data collected during *a*-Si:H nucleation and growth on the substrates. For the case of the Cr substrate, silicide formation during *a*-Si:H deposition was assessed by preparing a thin ~100 Å layer of *a*-Si:H on the substrate and then etching it away with atomic hydrogen generated thermally with a heated filament.[33] Complete removal of the *a*-Si:H yielded the same SE data for the uncovered Cr surface as was obtained prior to the *a*-Si:H deposition. As a result, no evidence of Cr silicide formation was found that would distort our interpretation of the *a*-Si:H nucleation and growth processes as presented in Sec. III C.

The real-time SE measurements were performed during the *a*-Si:H depositions using a rotating polarizer multichannel ellipsometer. The design, calibration, and operation of this instrument are described in detail elsewhere.[26,34,35] With this instrument, 128-point spectra can be collected from 1.4 to 4.5 eV with a minimum acquisition time of 40 ms. In the analyses described in Sec. III, we focused on the 57 data points from 2.48 to 4.00 eV, avoiding the low energy region where the *a*-Si:H films are weakly absorbing and the high-energy region where the experimental precision and accuracy are the lowest. For the *a*-Si:H depositions on SnO_2:F and μc-Si:H in which the roughness evolution is probed (Sec. III A), the acquisition and repetition times for such spectra were 3.2 and 15 s, respectively, the former corresponding to an average over 40 polarizer rotations. For the depositions on *c*-Si (Sec. III B) and Cr (Sec. III C) substrates in which the nucleation and coalescence processes are probed, the acquisition time was 0.16 s, corresponding to an average over two polarizer rotations. In these two cases, the repetition time for the collection of successive spectra was 0.8 s in the early stages of growth, but was extended in the later stages of growth. During the 0.16 and 0.8 s acquisition and repetition times, 0.2 and 1 Å of *a*-Si:H accumulated, respectively. The precision in (ψ, Δ) achievable on the Cr substrate at 2.48 eV for 0.16 and 3.2 s acquisition times is given by $(\delta\psi,\delta\Delta) \sim (0.015°,0.03°)$ and $(\delta\psi,\delta\Delta)\sim(0.003°,0.007°)$, respectively. The precision is defined as the standard deviation in the (ψ,Δ) values obtained in 120 repetitive measurements of a stable surface over a period of 30 min.

In the analysis of the full real-time SE data, one and two layer optical models for the growing *a*-Si:H are applied as shown in Fig. 2. Here, we provide an overview of these models. The one layer model is used to characterize the evolution of substrate-induced roughness on the opaque *a*-Si:H films (Sec. III A). In this analysis, the unknowns are the dielectric function of the bulk *a*-Si:H $\varepsilon_{\mathrm{sub}}=\varepsilon_b$, the void volume fraction in the roughness layer f_v, and the thickness of the roughness layer d_s. The dielectric function of the *a*-Si:H component in the surface layer is assumed to be the same as that of bulk *a*-Si:H, i.e., $\varepsilon_s=\varepsilon_b$. The two layer model is used

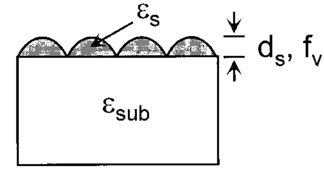

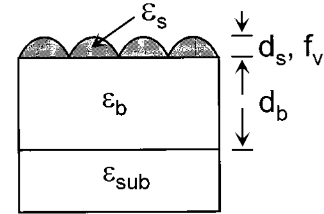

FIG. 2. One and two layer optical models applied in the analysis of real-time SE data. The one layer model is used to characterize discontinuous films during nucleation, as well as surface roughness evolution during the growth of opaque films. The two layer model is used to characterize the growth of transmitting films having rough surfaces.

to characterize the *a*-Si:H structural evolution on *c*-Si after initial nuclei make contact (Sec. III B). In this case, the unknowns include the bulk layer dielectric function ε_b, the thicknesses of the surface roughness layer d_s and the bulk layer d_b, and the void volume fraction f_v in the roughness layer. The dielectric function of the *a*-Si:H component in the roughness layer is again chosen to be the bulk layer dielectric function $\varepsilon_s=\varepsilon_b$. In the complete analysis of *a*-Si:H nucleation and growth on Cr, a transition from the one layer to two layer model is used (Sec. III C). For the one layer model, the dielectric function of the substrate $\varepsilon_{\mathrm{sub}}$ is known, and the unknowns include the dielectric function of the *a*-Si:H clusters $\varepsilon_s=\varepsilon_c$, the void volume fraction in the nucleating layer f_v, and the thickness of this layer d_s. For the two layer model, the unknowns are the same as in the case of growth on the *c*-Si substrate; however, the dielectric function of the *a*-Si:H component in the roughness layer is chosen to be either the bulk layer dielectric function $\varepsilon_s=\varepsilon_b$ or the cluster dielectric function $\varepsilon_s=\varepsilon_c$.

It is important to re-emphasize that because all substrate surfaces were maintained at a stable temperature of 200 ±2 °C throughout deposition,[36] all dielectric functions extracted and reported here are characteristic of the elevated temperature. As a result, it is not necessary to confine the analysis to a specific photon energy at which the dielectric function is only weakly dependent on temperature, as must be done if the process temperature is changing or if a reference dielectric function is employed for the final bulk film that was obtained at a different temperature than the stable substrate temperature.[37] In order to deduce the unknown information in our study, a global error minimization scheme is used in the analysis of the real-time SE data sets, which consist of 8–200 pairs of 57 point (ψ,Δ) spectra. This scheme involves numerical inversion to extract the unknown dielectric function, applied in conjunction with least squares regression analysis to extract the photon energy-independent microstructural parameters. Although the general procedure

is described elsewhere,[38,39] abbreviated descriptions are provided in Sec. III for the three specific cases relevant to this investigation.

Finally, we note that for additional *a*-Si:H depositions on SnO_2 and Cr surfaces, the polarized reflectance R was measured simultaneously with the (ψ,Δ) spectra as described elsewhere.[40] In both cases, R can be closely fit using the dielectric functions and microstructural parameters extracted in best fits to the (ψ,Δ) spectra alone. As a result, we conclude that non-specular scattering losses are undetectable. This in turn shows that any macroscopic roughness components are less than 10 Å in amplitude (full width of a Lorentzian distribution for the surface height profile),[41] and supports an interpretation of the data of Sec. III in terms of microscopic roughness alone. The overall consistency in the analysis of (ψ,Δ) and R also supports the surface roughness layer optical model in which the Fresnel boundary conditions are applied at the layer interfaces.

III. RESULTS

A. Effective medium theories of microscopic roughness evolution on *a*-Si:H

In our first assessment of EMT's, we have studied the evolution of the surface roughness layer on opaque *a*-Si:H deposited on microscopically rough substrates. In this film growth process, the substrate surface is conformally covered by the growing *a*-Si:H film. The substrate-induced roughness on the *a*-Si:H decays exponentially with increasing bulk layer thickness for the in-plane spatial periods of the surface profile that are shorter than the diffusion length of Si-bearing precursors on the growing *a*-Si:H surface.[42,43] Measurement of the decay constant has provided an estimate of the surface diffusion length of the precursors.

Optical analysis of the film growth process involves solving the one layer problem described in Sec. II. In the one layer problem, we must extract (i) the *a*-Si:H bulk layer dielectric function $\varepsilon_b = \varepsilon_{1b} + i\varepsilon_{2b}$, (ii) the time evolution of the surface roughness layer thickness $d_s(t)$, and (iii) the assumed constant void volume fraction f_v in the surface roughness layer. The spectra in ε_b and the value of f_v are substituted into the selected EMT to generate the dielectric function of the roughness layer. Because the overall analysis is performed in the opaque regime, the bulk layer thickness $d_b(t)$ does not enter into the problem.

A time t' is selected near the middle of the analysis range at a bulk layer thickness of ~3500 Å. At t' the ellipsometric spectra (ψ,Δ) are analyzed to deduce ε_b, which is used in a global error minimization procedure applied to the time-dependent data set. This data set spans the bulk layer thickness range where the *a*-Si:H is opaque for photon energies $\geqslant$ 2.48 eV. We use the ranges of 2500–4300 Å and 2900–4300 Å for *a*-Si:H growth on the μc-Si:H and SnO_2:F substrates, respectively. The steps of this analysis procedure are described as follows. First, initial guesses are made for the fixed void volume fraction f_v and the roughness layer thickness $d_s(t')$ at the selected time t'. With these guesses, the (ψ,Δ) spectra at t' are subjected to a numerical inversion routine that yields a trial dielectric function for the bulk *a*-Si:H film. This trial dielectric function is utilized in a least squares regression analysis of the (ψ,Δ) data set to extract

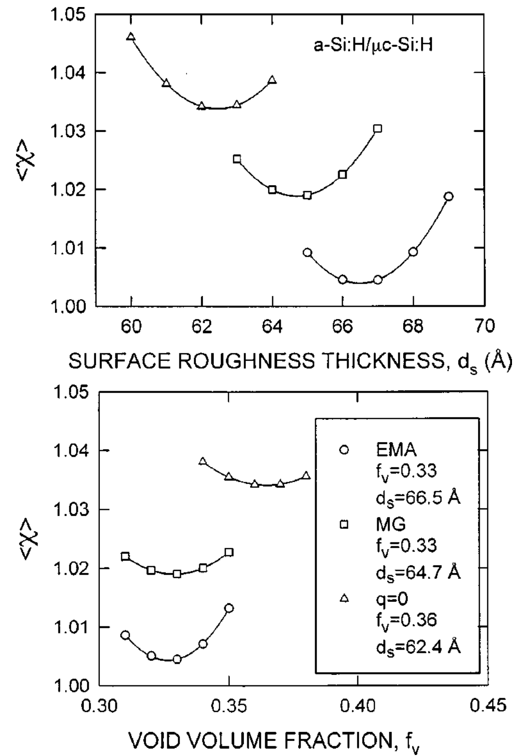

FIG. 3. Illustration of the procedure applied to identify the best-fit surface roughness layer thickness d_s and the roughness layer void volume fraction f_v in a one layer optical model at a selected time corresponding to the bulk layer thickness of ~3500 Å during the deposition of opaque a-Si:H on a rough μc-Si:H film. Here the average biased estimator of the mean square deviation $\langle\chi\rangle$ is plotted versus the trial value for d_s at fixed f_v (top) and versus the trial value of f_v at fixed d_s (bottom). The fixed values are selected as those that minimize $\langle\chi\rangle$. Three different EMTs are employed to determine the roughness layer dielectric function, the $q=0$ limit (triangles), EMA (circles), and MG (squares).

$d_s(t)$ and the time dependence of the biased estimator of the mean square deviation $\chi(t)$ between the experimental data and the best fit.[44] The value of the biased estimator averaged over time, denoted $\langle\chi\rangle$, provides a measure of the global goodness of the fit and, thus, allows one to assess the validity of the initial guesses $\{d_s(t'),f_v\}$. In the analysis, the initial guesses are varied over a two-dimensional grid in an attempt to minimize $\langle\chi\rangle$. The values of the initial guesses that minimize $\langle\chi\rangle$ are assumed to be correct, and this in turn leads to the correct dielectric function by inversion, and the correct $d_s(t)$ variation, along with the 95% confidence limits.

As described in Ref. 44, for the biased estimator formulation of the error function, the individual squared deviations between the experimental and best-fit tan ψ and cos Δ values at each photon energy are divided by an estimate of the combined random and systematic mean-square errors in the experimental values at the corresponding photon energy. Thus, when $\langle\chi\rangle$ is on the order of unity, we can conclude that the fit is as best as can be expected within consideration of the experimental errors and that the model leading to $\langle\chi\rangle=1$ is acceptable.

Figure 3 shows results for $\langle\chi\rangle$ corresponding to orthogonal cuts in the two-dimensional parameter space of the trial $\{d_s(t'),f_v\}$ values for the analysis of *a*-Si:H growth on

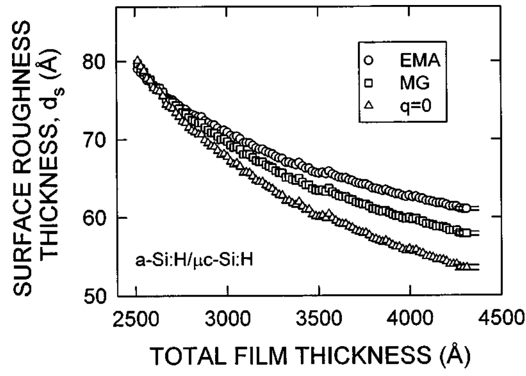

FIG. 4. Evolution of the surface roughness layer thickness d_s versus the extrapolated total film thickness during the growth of a-Si:H on a rough substrate film of μc-Si:H using the three EMT's that yield nonzero solutions for d_s and f_v in Fig. 3. Over the thickness ranges shown, the growing a-Si:H is fully opaque for photon energies greater than 2.48 eV.

μc-Si:H. These results are typical of the data obtained for growth on both types of substrates, rough μc-Si:H and SnO_2. The cuts chosen in Fig. 3 intersect at the $\{d_s(t'),f_v\}$ solution yielding minimum $\langle\chi\rangle$. In this plot, data for only three of the five EMT's are shown, EMA (circles), MG (squares), and the $q=0$ limit (triangles). Well-defined minima in two-dimensional parameter space are obtained that allow one to identify the best choice of $\{d_s(t'),f_v\}$. This in turn allows one to extract the dielectric function ε_b of the bulk layer and the surface roughness thickness evolution $d_s(t)$. For the other two EMT's the LL and the $q=1$ limit, however, the minima in $\langle\chi\rangle$ appear at $d_s(t')=0$ for depositions on both types of substrates. For these EMT's, the $\langle\chi\rangle$ values are ~50% higher than the minima for the other three EMT's in Fig. 3.

It is important to note that we observe precisely the same trends in the solutions for a-Si:H depositions on both rough μc-Si:H and SnO_2 substrates, thus supporting the significance of the results. Specifically, the EMA yields the best overall fit whereas the fits using the MG and $q=0$ limit are slightly worse. Although the improvement in $\langle\chi\rangle$ provided by the EMA in Fig. 3 appears inconsequential (~1–3%), it is consistent as a function of the deposition time, with the largest improvement in χ occurring at the extremes of the analysis ranges. For example, 5–10% improvements in the fits are obtained when the EMA is used in place of the $q=0$ limit for the 40–80 Å surface roughness layers at the start and end of the analysis ranges for the a-Si:H depositions on μc-Si:H and SnO_2:F (see, for example, Fig. 4). The solutions for f_v also reveal similar trends for both depositions, namely, $f_v=0.33$ for the EMA and the MG EMT, and $f_v=0.36$ for the $q=0$ limit. For both depositions, the EMA yields the largest roughness thicknesses, whereas the MG and $q=0$ limit yield successively lower thicknesses.

Figure 4 shows the surface roughness evolution d_s versus the extrapolated total film thickness during a-Si:H growth on the μc-Si:H substrate, for the three EMT's that yield the non-zero solutions of Fig. 3. For depositions on both substrates, the best-fitting EMA provides the overall largest roughness layer thickness, which decays from 80 to 60 Å for the μc-Si:H substrate (see Fig. 4) and from 50 to 44 Å for the SnO_2:F substrate. The maximum difference for the roughness thickness solutions using the three different EMT's is 7 Å for the μc-Si:H substrate (see Fig. 4) and 3 Å for the SnO_2:F substrate. Figure 5 shows the best-fit dielectric functions at 200 °C deduced from the data set obtained for the SnO_2:F substrate using the three different EMT's of Figs. 3–4. Also included are the results deduced using the LL and the $q=1$ limit, in which case the roughness thickness that minimizes $\langle\chi\rangle$ is zero. Thus, the dielectric function for these latter two EMT's is equal to the measured pseudodielectric function. This solution can be ruled out, however, because of the overall poorer fits, as noted above, and also because AFM reveals that the film surface is in fact considerably rough (see Sec. III D). In Fig. 5, the largest overall amplitude for the dielectric function is obtained for the EMA with a maximum ε_{2b} of 28.4.

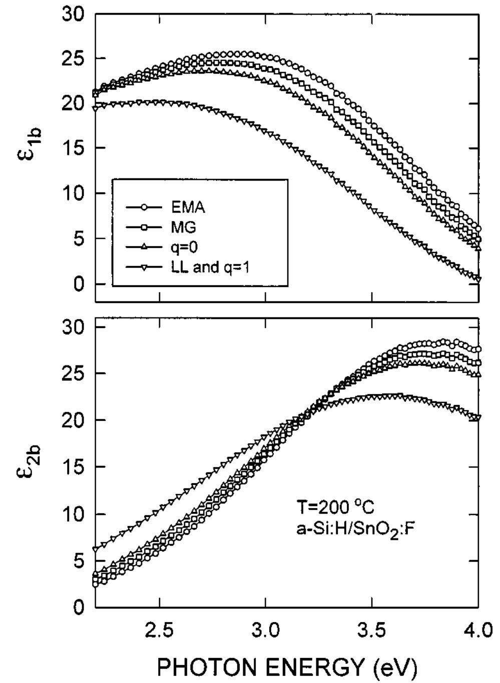

FIG. 5. Best-fit bulk a-Si:H dielectric functions at 200 °C deduced from real-time SE data collected during the growth of opaque a-Si:H on a rough film of SnO_2:F using five different EMT formulations. In all cases, a one layer optical model is used. For the $q=1$ limit and the LL EMT, the best-fit surface roughness layer thickness is zero. Thus, the deduced dielectric function is equal to the measured pseudodielectric function.

B. Effective medium theories for the coalescence of *a*-Si:H

In the second assessment of effective medium theories, we have studied the roughness layer evolution for a-Si:H after initial nuclei make contact. In this case, the substrate is a c-Si wafer coated with a native oxide layer, a structure having atomic level smoothness. As a result, the roughness that forms on the a-Si:H is characteristic of the nucleation process and is not substrate induced. During nuclei coalescence, the nucleation-induced roughness layer thickness is rapidly damped to a stable value after ~50 Å bulk layer thickness. This behavior is in contrast to the very slow surface smoothening that occurs over a bulk thickness range of

1000–2000 Å for the substrate-induced roughness (see Sec. III A). The shorter relaxation time for nucleation-induced roughness is likely to arise from shorter in-plane spatial periods for the surface profile.[42,43] The degree of surface smoothening during coalescence of *a*-Si:H clusters on *c*-Si substrates has been found to correlate closely with the electronic quality of the resulting material.[45] For example, the highest efficiency and highest stability *p-i-n* solar cells are obtained under conditions in which *a*-Si:H intrinsic-layer growth is performed at the highest possible H_2-dilution of SiH_4 while ensuring that the film does not develop microcrystallinity. Under precisely these conditions, a maximum smoothening effect occurs during coalescence as observed from depositions on *c*-Si substrates.[46]

Because the bulk *a*-Si:H layer in this second study is very thin and transmits light to the substrate, the two layer optical analysis of Sec. II must be performed. In this analysis, we must extract (i) the bulk layer dielectric function $\varepsilon_b = \varepsilon_{1b} + i\varepsilon_{2b}$, (ii) the time evolution of the bulk layer thickness $d_b(t)$, and (ii) the time evolution of the surface roughness layer thickness $d_s(t)$. Because of the additional complexity of this problem, the volume fraction of void in the roughness layer is fixed at $f_v = 0.5$. This is the value typically chosen for thin roughness layers in the absence of additional information; however, further justification for this choice will come from the results of Sec. III C.

A time t' is selected at the end of the analysis range at a bulk layer thickness of ~200 Å. At t' the ellipsometric spectra (ψ,Δ) are analyzed to deduce ε_b which is used in a global error minimization procedure applied to the time-dependent data set as described in Sec. III A. In this case, the data used for error minimization were collected over the bulk layer thickness range from 0 to 200 Å. First, initial guesses are made for the bulk and surface roughness layer thicknesses $d_b(t')$ and $d_s(t')$, respectively. With these guesses, the (ψ, Δ) spectra at t' are subjected to numerical inversion in order to generate a trial dielectric function for the bulk *a*-Si:H film. This trial dielectric function is utilized in a least squares regression analysis of the time-dependent data set, yielding $d_b(t)$, $d_s(t)$, and $\chi(t)$. As in Sec. III A, the value of the time-averaged biased estimator $\langle\chi\rangle$ provides a measure of the global goodness of the fit and allows one to assess the validity of the initial guesses $\{d_b(t'),d_s(t')\}$. The values of the initial guesses that minimize $\langle\chi\rangle$ are assumed to be correct. This in turn leads to the correct dielectric function by inversion and the correct $d_b(t)$ and $d_s(t)$ variations, along with the 95% confidence limits.

Figure 6 shows results for $\langle\chi\rangle$ obtained in the analysis of *a*-Si:H growth on *c*-Si. Data in $\langle\chi\rangle$ are shown along two orthogonal cuts in the parameter space of the trial $\{d_b(t'),d_s(t')\}$ values. In this plot, the results for the five different EMT's are shown, EMA (open circles), MG (open squares), the $q=0$ limit (open triangles), LL (filled squares), and the $q=1$ limit (filled circles). All results in Fig. 6 show well-defined minima that allow one to identify the best choice of $\{d_b(t'),d_s(t')\}$, when each EMT is applied in turn. The existence of the minimum allows one to extract ε_b, $d_b(t)$, and $d_s(t)$. The results of Fig. 6 show that the EMA yields the best overall fit to the full data set, with the LL and MG a close second and third best. Considering the results for the five EMT's the deduced bulk layer thickness ranges from 191 to 199 Å, and the deduced surface roughness layer thicknesses ranges from 13 to 19 Å.

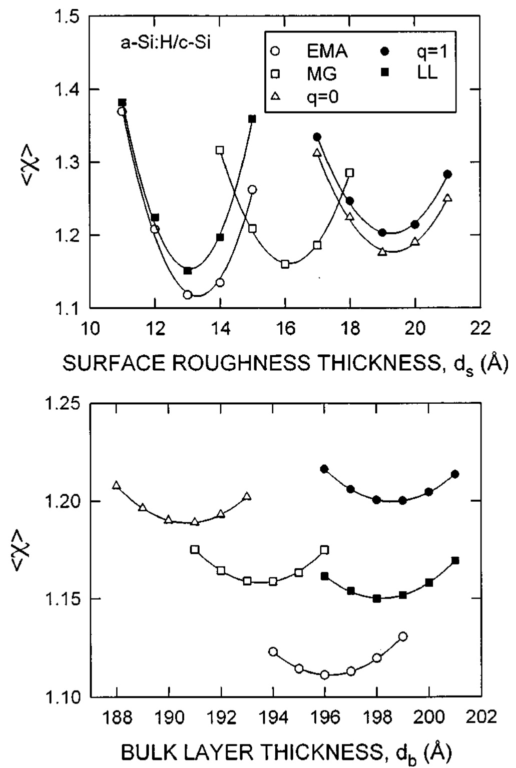

FIG. 6. Illustration of the procedure applied to identify the best-fit bulk layer thickness d_b and surface roughness layer thickness d_s in a two layer optical model at a selected time, corresponding to d_b~200 Å during the deposition of *a*-Si:H on a smooth *c*-Si substrate. Here the average biased estimator of the mean square deviation $\langle\chi\rangle$ is plotted versus the trial value for d_s at fixed d_b (top) and versus the trial value of d_b at fixed d_s (bottom). The fixed values are selected as those that minimize $\langle\chi\rangle$. Five different EMT's are employed to determine the roughness layer dielectric function in the analysis.

Figure 7 shows the time evolution of the bulk and surface roughness layer thicknesses, and the quality of the fit during the first minute of *a*-Si:H growth on the *c*-Si wafer, obtained by applying each of the five different EMT's. This figure shows that the dominant improvement in the fit for the EMA occurs over the time range of 5–30 s . In fact, the improvement in χ over this range is much larger than is indicated by the minimum $\langle\chi\rangle$ values of Fig. 6. For example, when $d_b = 10$ Å and $d_s = 14$ Å, the EMA provides a 20–30% improvement in fitting over the MG, LL, and $q=0$ limit and an 80% improvement over the $q=1$ limit. With increasing bulk layer thickness, however, the improvement provided by the EMA becomes much less significant and this reduces the differences between the $\langle\chi\rangle$ values.

For all EMT's, the surface roughness characteristics in Fig. 7 are parallel. Even though the thickness at which nuclei make contact (where d_b increases above one monolayer or ~2.5 Å) ranges from a maximum of 23 Å for the $q=0$ limit to a minimum of 16 Å for the LL, the smoothening effect during coalescence, defined as $d_s(d_b = 2.5\,\text{Å}) - d_s(d_b = 50\,\text{Å})$, is essentially independent of the selected EMT. The time dependences of the bulk layer thickness are parallel as well for all five EMT's; only three are shown in Fig. 7 for

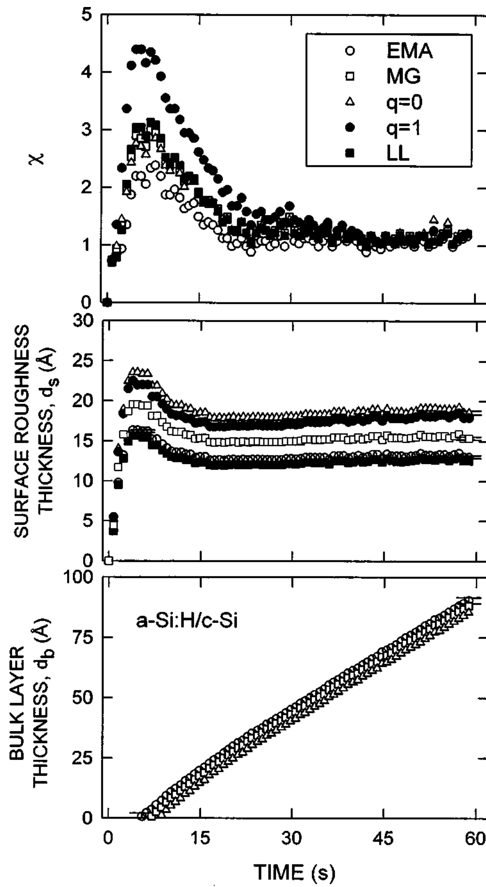

FIG. 7. Time evolution of the bulk layer thickness d_b (bottom), the surface roughness layer thickness d_s (center), and the biased estimator of the mean square deviation χ (top) during the first minute of *a*-Si:H growth on *c*-Si, obtained by applying each of the five different EMT's. In this case, the dielectric function of the surface layer was obtained from the EMT assuming a 0.5/0.5 volume fraction mixture of bulk *a*-Si:H/void.

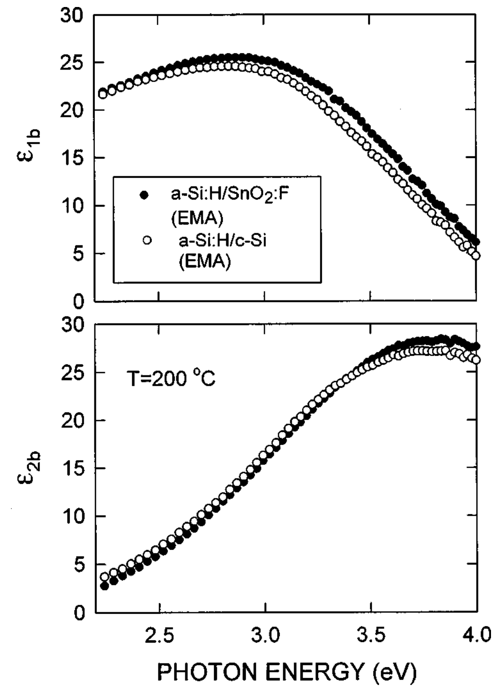

FIG. 8. Bulk layer dielectric functions at 200 °C for *a*-Si:H deduced using one and two layer models for the growth of *a*-Si:H on SnO_2:F and *c*-Si substrates, respectively. These results were obtained at bulk layer thicknesses of ~3500 Å for the SnO_2 substrate and ~200 Å for the *c*-Si substrate. The EMA has been applied in the optical modeling to determine the sample microstructure.

clarity. The slightly higher deposition rate in the first 10 s of bulk layer growth is attributed to the incorporation of the surface roughness material as part of the bulk material upon smoothening during coalescence. After coalescence ($t > 30$ s), the deposition rate is constant and independent of the chosen EMT. Figure 8 shows the bulk *a*-Si:H dielectric functions at 200 °C deduced using the EMA in the first and second EMT assessments for the SnO_2:F and *c*-Si substrates, respectively. Considering the sensitivity of ε_b to the surface correction procedure, the agreement is quite good. In fact, the difference in Fig. 8 can be attributed to errors in the deduced surface roughness thickness at the level of less than ±0.5 monolayer (±1 Å).

C. Complete analysis of nucleation and coalescence in *a*-Si:H

In a third assessment of the EMT's, we consider the cluster stage of *a*-Si:H nucleation when the one layer model of Sec. II is appropriate. This model is expected to be valid in the first ~20 Å of "surface roughness layer" growth (see Fig. 7 results for d_s) prior to the formation of the bulk layer. For the deposition of this third assessment, however, the *c*-Si substrate of Sec. III B is replaced by a metallic Cr substrate. With such a substrate, higher sensitivity in the analysis of the dielectric functions of ultrathin layers are obtained. In this analysis, a global error minimization procedure is used in which we extract (i) the dielectric function ε_c of the cluster component of the nucleating layer, i.e., excluding the void component, for the thickness at which the nuclei make contact, (ii) the time dependence of the cluster layer thickness $d_s(t)$, and the time dependence of the void volume fraction in the layer $f_v(t)$. Very poor sensitivity is expected in determining f_v independently due to correlations between this parameter and ε_c. We also note that ε_c will be different in general from the bulk layer dielectric function ε_b, because of the differences in the concentrations of Si-Si and Si-H bonds within the clusters relative to the concentrations in the bulk film. In fact, measurements of the dielectric function continuously versus cluster film thickness has allowed us to extract the optical gap, which provides information on the evolution of the composition of the clusters.[28]

The specific analysis procedure is essentially the same as that of Secs. III A and III B. We seek a minimum in the error function $\langle\chi\rangle$ for guesses of $f_v(t')\sim 0.5$ and $d_s(t')\sim 20$ Å where t' is selected to be the time at which the nuclei make contact. This contact point is obtained in a preliminary analysis performed on the data set similar to that described in Sec. III B for the *c*-Si substrate (see Fig. 7). Fits to ellipsometric spectra (ψ,Δ) collected for $t<t'$ are used to establish the time-averaged error function $\langle\chi\rangle$. Figure 9 shows the minima identified in the error function $\langle\chi\rangle$ based on orthogonal cuts in parameter space (as in Figs. 3 and 6). Well-defined minima as a function of d_s are observed from 16 to 17 Å using the EMA, MG, and the $q=0$ limit. Much weaker minima for f_v are observed from 0.48 to 0.50 for the three

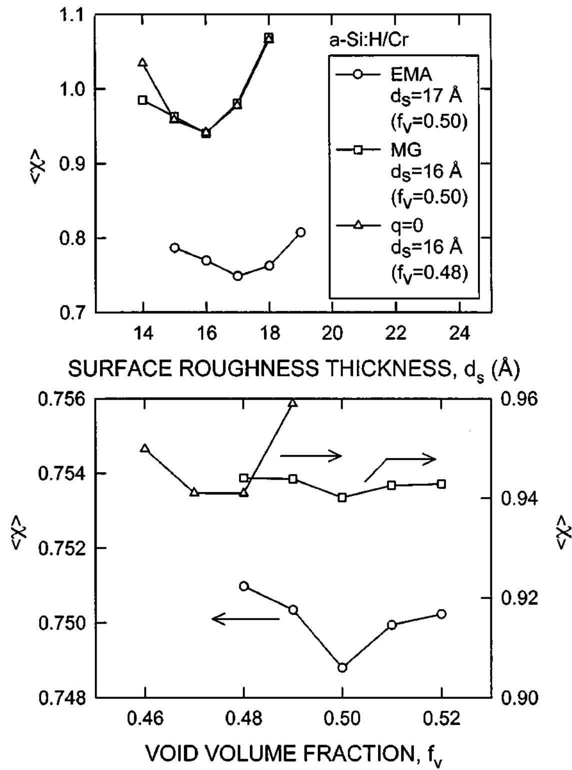

FIG. 9. Illustration of the procedure applied to identify the best-fit nucleating layer thickness d_s and its void volume fraction f_v in a one layer optical model at a selected time, corresponding to a nucleating layer thickness of 17 Å during the initial growth of *a*-Si:H on a Cr substrate. Here the average biased estimator of the mean square deviation $\langle\chi\rangle$ is plotted versus the trial value for d_s at fixed f_v (top) and versus the trial value of f_v at fixed d_s (bottom). The fixed values are selected as those that minimize $\langle\chi\rangle$. Three different EMT's are employed to determine the nucleating layer dielectric function.

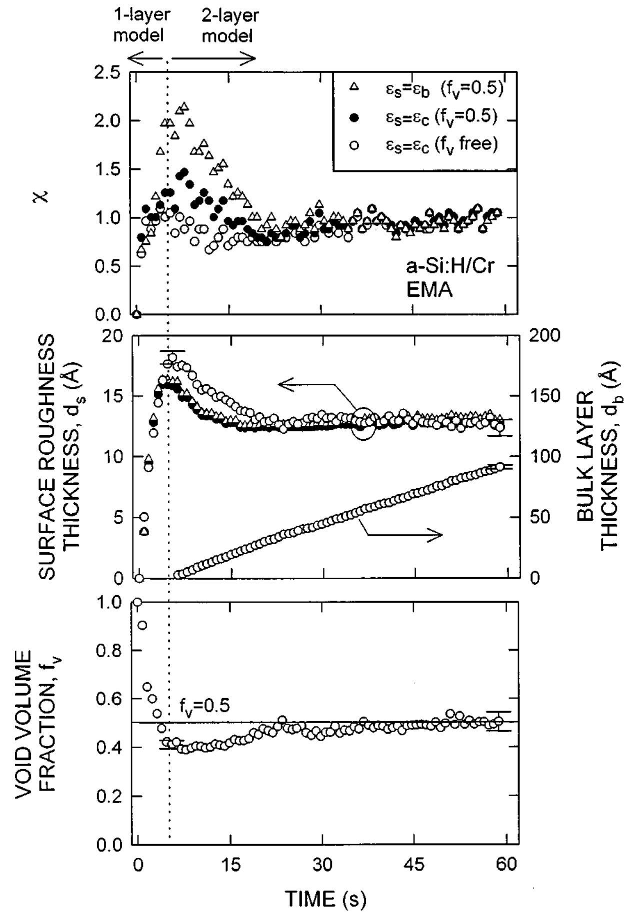

FIG. 10. Evolution of the nucleating and surface roughness layer void volume fraction f_v (bottom), the surface roughness and bulk layer thicknesses d_s and d_b (center; left and right scales), and the biased estimator of the mean square deviation χ (top) obtained in one and two layer analyses of real-time SE data collected during the nucleation and growth of *a*-Si:H on Cr. For the open circles, the EMA was used to determine the dielectric function of the nucleating and roughness layers, using the dielectric function of the *a*-Si:H clusters from Fig. 11. In this case, the void volume fraction f_v is a free parameter. For the solid circles, the same EMA approach is used, but f_v is fixed at 0.5. For the triangles, the dielectric function of *a*-Si:H bulk material is used instead of that of *a*-Si:H clusters, and f_v is fixed at 0.5.

EMT's. In contrast, no minima versus d_s or f_v could be identified using the LL and $q=1$ limit formulations. Figure 9 also shows that the EMA provides a 20–25% overall improvement in $\langle\chi\rangle$ over the MG and $q=0$ limit, similar to that obtained in the early stages of *a*-Si:H growth on *c*-Si in Fig. 7.

The results for the best-fit evolution of d_s, f_v, and χ using the EMA are given in Fig. 10 as the open circles in each one of the panels for the one-layer time regime. For the two layer regime, we used an approach similar to that described in Sec. III B. In this approach, we focus on the spectra collected when the bulk layer thickness is ~200 Å, and perform a three parameter (d_b, d_s, f_v) error minimization procedure at this selected time. Two differences are incorporated into the analysis of Fig. 10 compared to the analysis of Fig. 7 in Sec. III B. First, the dielectric function of the surface layer is modeled as a mixture of *a*-Si:H and void, but with the dielectric function for the *a*-Si:H component chosen as ε_c from the analysis of Fig. 9 (not ε_b as in Fig. 7). Second, f_v is used as a free parameter in the error minimization at $d_b=200$ Å, and it is also used as a free parameter in the least squares regression analysis versus time. This becomes possible owing to the higher sensitivity provided by the Cr substrate. In Fig. 10 (bottom), f_v is observed to increase from 0.4 to 0.5 during the coalescence and growth processes. Thus, the selection of $f_v=0.5$ in the analysis of Sec. III B is reasonable.

Also shown in Fig. 10 for comparison are the results of the full analysis when these two differences are not incorporated into the analysis. First, the results given by the closed circles are deduced assuming f_v is fixed at 0.5 throughout the one and two layer modeling regimes. Second, the results given by the triangles are deduced assuming that f_v is fixed at 0.5 and that the dielectric function of the *a*-Si:H component in the surface layer is chosen as $\varepsilon_s=\varepsilon_b$. The latter simplified version of the model is identical to that used to generate the results of Fig. 7 for *a*-Si:H growth on the *c*-Si substrate. The incorporation of either one or both simplications in the model leads to a significant increase in $\chi(t)$ in the first 20 s of the growth process. This behavior demonstrates that the cluster and surface roughness *a*-Si:H compo-

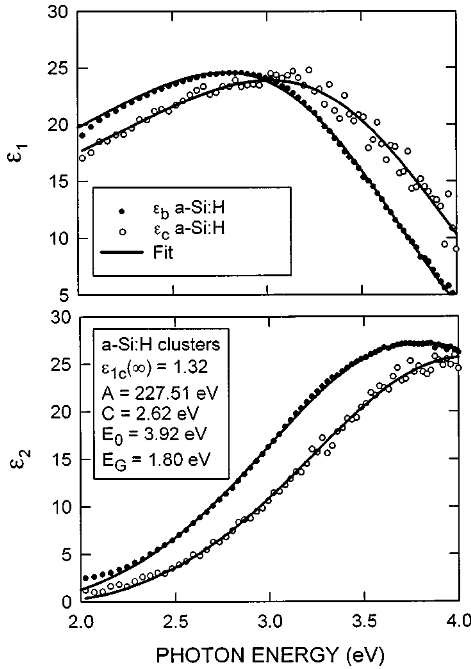

FIG. 11. The dielectric function of the a-Si:H clusters ($d_s = 17$ Å) deduced from real-time SE data collected during a-Si:H nucleation on a Cr substrate (open circles). These results were obtained in the analysis of Fig. 9 using the EMA. Also shown is the dielectric function of the bulk layer ($d_b \sim 200$ Å) for a-Si:H deposited on c-Si as reproduced from Fig. 8 (closed circles). The solid lines are fits to the Tauc-Lorentz formula for the dielectric function of an amorphous semiconductor. The deduced parameters are given for the a-Si:H cluster dielectric function.

nents exhibit a different dielectric function than the bulk in the case of the nucleating and coalescing a-Si:H films. If this feature is not included in the optical model, then the quality of the fit degrades by ~50% for films consisting of $d_b = 10$ Å and $d_s = 15$ Å. This problem also accounts for the peak in $\chi(t)$ for the EMA at ~6 s in Fig. 7. In the later stage of growth, i.e., for bulk layers greater than 50 Å, this problem disappears and the quality of the fit depends much less strongly on the a-Si:H component dielectric function used for the surface roughness layer.

Figure 11 depicts the dielectric function ε_c at 200 °C obtained in the analysis of Fig. 9 using the EMA. Also shown is the dielectric function of the bulk a-Si:H layer deposited on c-Si, as reproduced from Fig. 8. The higher noise level for the nucleating layer component dielectric function arises because it was extracted for a 17 Å-thick cluster film with a void volume fraction of $f_v = 0.48$, whereas the bulk layer dielectric function was extracted from a 200 Å-thick film. The solid lines in the figure are best fits using the Tauc-Lorentz model for the dielectric function of an amorphous semiconductor.[47] The free parameters of this model are given in the inset for the a-Si:H clusters. The parameter A is the overall amplitude, C is the Lorentz oscillator broadening parameter, E_0 is the oscillator resonance energy, E_G is the Tauc optical gap, and $\varepsilon_{1c}(\infty)$ is the constant contribution to ε_{1c}. For both dielectric functions, excellent fits using this model are obtained. The primary difference between the a-Si:H cluster and bulk dielectric functions is the overall 0.2 eV shift to higher energy for the former, attributed to a

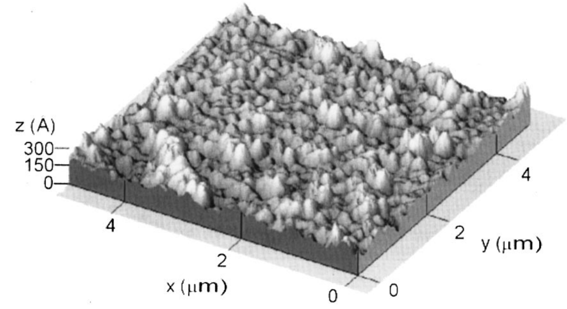

FIG. 12. Atomic force microscopy image (5×5 μm^2) for the final 4300 Å-thick a-Si:H film deposited at 200 °C on a microscopically rough SnO_2:F substrate.

higher H content in the a-Si:H clusters and surface layer. In fact, using the correlation obtained for bulk a-Si:H films of different H contents, the observed increase in gap is consistent with an increase in H content from ~10 to 25 at. %.[48]

D. Correlations with atomic force microscopy

The a-Si:H films prepared onto smooth c-Si and rough SnO_2:F were studied *ex situ* by AFM in the tapping mode. Since the a-Si:H surfaces are expected to remain H terminated even for a time after removal from the deposition system and possibly during AFM measurement, the tapping mode was used in order to avoid any modification of the surface by a contacted probe tip. Figure 12 shows a 5×5 μm^2 image for the a-Si:H on SnO_2:F whose final roughness layer is 44 Å thick, as deduced from real-time SE with the EMA analysis. The root-mean square (rms) roughness computed from this image was found to be 31 Å, significantly lower than the roughness thickness measured from real-time SE at the end of deposition. Figure 13 shows the final roughness layer thickness from real-time SE studies of different amorphous semiconductor films obtained using the

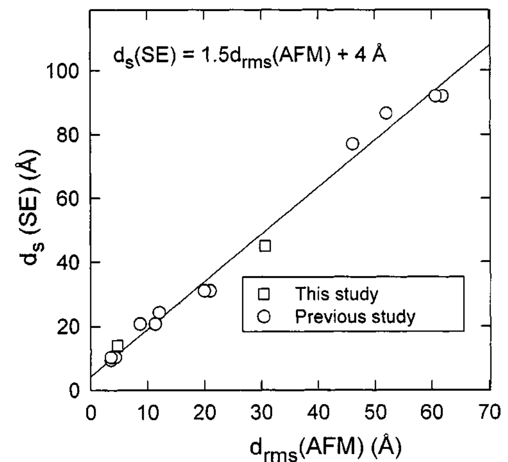

FIG. 13. Final roughness layer thickness on a-Si:H films deduced from real-time SE measurements using the EMA analysis, plotted versus the rms roughness deduced from 5×5 μm^2 atomic force microscopy images such as that in Fig. 12. The square data points were obtained in this study, whereas the open circles were obtained in a previous study of different amorphous semiconductor films. For $d_s < 40$ Å the substrates were smooth c-Si wafers, and for $d_s > 40$ Å the substrates were microscopically rough SnO_2:F films.

EMA in the data analysis, plotted versus the rms roughness from 5×5 μm^2 AFM images measured *ex situ*. An excellent linear correlation is observed, and the data of this study (squares) follow the same trend as those reported earlier (circles).[19] The correlation is best fit by the relationship $d_s=1.5d_{\rm rms}({\rm AFM})+4$ Å.

The slope and intercept in this relationship have reasonable explanations.[19] From an analysis of the AFM bearing ratio profile, the slope of 1.5 is found to imply that *a*-Si:H protrusions exist above the upper ambient/roughness interface and void protrusions exist below the lower roughness/bulk interface, both at the level of 5–7% of the total volume of the optically deduced roughness layer. This simply means that the SE measurement is insensitive to the presence of protrusions at this concentration level. The nonzero intercept on the other hand, may have two explanations. First, it may represent the amplitude of roughness components below the spatial resolution of AFM. Alternatively, the 4 Å intercept may represent the thickness of a more heavily hydrogenated surface layer that is interpreted as roughness by SE because of its lower Si-Si bond packing density, but not by AFM because of its apparent homogeneity on the 50–100 Å lateral resolution scale of the microscope. Evidence for such a layer also appears in the measured dielectric function for the *a*-Si:H clusters in Sec. III C.

IV. DISCUSSION

An important observation from the analyses of Figs. 3, 6, and 9 is the consistent improvement in fitting provided by the EMA over the other one-parameter EMT's for each of the applications in which EMT's are traditionally used. These applications include nucleating layers consisting of discontinuous clusters and surface roughness layers induced either by nucleation or by underlying substrate surface roughness. In general, the excellent correlation between the roughness layer thickness from real-time SE and AFM in Fig. 13 supports the validity of an EMT analysis approach in which the rough surface region is replaced by a layer having an effective dielectric function. The lack of SE-AFM correlations along with the poorer fits for the LL and $q=1$ limit of the EMT are sufficient to rule out these formulations. The correlation of Fig. 13, however, cannot be used to support the EMA over the MG and $q=0$ limit of the EMT, owing to the uncertainties in the slope and intercept of the correlation. For example, similarly good correlations as in Fig. 13 can be obtained for the MG and the $q=0$ limit, but the slope and intercept are observed to decrease and increase, respectively, in the order EMA, MG, $q=0$. In the next three paragraphs, we discuss the results and relative sensitivities of our three different EMT assessments of Secs. III A–III C.

For substrate-induced surface roughness evolving on an opaque bulk film, as analyzed in Figs. 3–5, the LL and $q=1$ limit of the EMT can be ruled out whereas the three other simple EMT's, namely the EMA, MG, and the $q=0$ limit all provide relatively good descriptions of the data with minima in $\langle\chi\rangle$ differing by no more than $\sim$3%. The origin of this behavior can be understood on the basis of Fig. 1, where it can be seen that the LL EMT and the $q=1$ limit yield dielectriclike responses for the microscopic mixture that defines the roughness layer. In contrast, the EMA, MG, and $q=0$ limit yield responses paralleling that of *a*-Si:H. It would seem reasonable that if any one of the latter three responses provided a good description of the data, the other two would as well. Only small adjustments in roughness layer thickness or void fraction would be required to compensate for the increasing magnitude of the effective dielectric function in the order EMA, MG, and $q=0$. In fact, the tendency in Fig. 3 for the best-fit void fraction to increase and the roughness layer thickness to decrease in the order EMA, MG, and $q=0$ illustrates this compensation effect.

The analysis of the evolution of substrate-induced surface roughness on an opaque film can narrow the range of possible EMT's to the EMA, MG, and the $q=0$ limit. Analysis of the nucleation-induced roughness for the 200 Å *a*-Si:H deposited on *c*-Si provides stronger support for the EMA. Although all EMT formulations yield minimum $\langle\chi\rangle$ values that are within $\sim$10% of one another, in the initial stages of growth, i.e., for $d_b<50$ Å, the EMA provides as much as a 20% improvement over the best alternative, which is the $q=0$ limit. In the later stages of growth, the dielectric nature of the LL and $q=1$ surface roughness responses can be compensated by erroneous increases in the bulk layer thicknesses by 2–3 Å. Thus, in this regime all EMT formulations can provide satisfactory fits, and the larger data set here has a tendency to suppress the differences in $\langle\chi\rangle$ arising in the initial stage of growth.

The nucleation of *a*-Si:H on Cr provides additional definitive evidence of the superiority of the EMA. The reason for this is that the Cr substrate provides strong optical contrast to the nucleating layer, and thus high sensitivity to the cluster dielectric function in the initial stages of growth. As noted in Sec. III (C) the EMA provides an average 20–25% improvement in $\langle\chi\rangle$ over the MG and $q=0$ limit for reasonable best-fit values of f_v in the range of 0.48 to 0.50. In this data analysis problem, the differing magnitudes of the composite dielectric functions of Fig. 1 are compensated by different deduced dielectric functions for the *a*-Si:H clusters. The similarity of the shapes of ε_c and ε_b in Fig. 11, together with the fact that ε_c can be closely fit using the Tauc-Lorentz model, provide support for the validity of the EMA analysis of Fig. 9. The Tauc-Lorentz model is one of the simplest Kramers-Kronig consistent descriptions found to fit the dielectric functions of a wide variety of amorphous semiconductors.[47] In addition, the higher H content in the nucleating layer component, as deduced from the shift to higher energies in the dielectric response and optical gap, is qualitatively consistent with several studies based on *in situ* infrared reflectance and SE measurements of *a*-Si:H nucleation and growth.[49–51] In fact, recent quantitative real time infrared reflectance measurements of 16 Å-thick *a*-Si:H cluster films on *c*-Si substrates show a total H content of $\sim$25 at. %, in comparison with 10 at. % for the bulk *a*-Si:H.[51] This result is in agreement with our interpretation of Fig. 11 and suggests that the shift in the dielectric function and optical gap to higher energy for the clusters can be fully accounted for by the increase in H content. Finally, the agreement between optical and infrared spectroscopic measurements of cluster composition provide additional support for a model of the discontinuous clusters in terms of a discrete layer in which the Fresnel boundary conditions are applied at the layer interfaces.

Next, we discuss the significance of the best-fit volume fractions used in the EMA. For *a*-Si:H films ranging in bulk layer thickness from 10 to 200 Å, the best-fit void volume fractions in the nucleation-induced roughness range from 0.4 to 0.5. In contrast, for thick *a*-Si:H layers, the best-fit void volume fractions in the substrate-induced roughness are considerably lower, 0.30 to 0.35. Although AFM measurements have revealed no significant differences in the shape or symmetry of the bearing ratio between nucleation-induced and substrate-induced roughness, the AFM measurement is not definitive since it may not detect the deepest voids in the surface structure whose spatial periods are the shortest. Two differences in the nature of the nucleation-induced and substrate-induced roughness layers may account for the different void volume fractions. First, AFM does indicate differences in the aspect ratio of the roughness for thinner nucleation-induced roughness (10–15 Å) and the much thicker substrate-induced roughness (40–80 Å). The latter has a larger in-plane to out-of-plane feature size ratio. The stronger dielectric function magnitude for the thicker substrate-induced roughness may reflect this difference in aspect ratio. Alternatively, for the thinner nucleation-induced roughness layers (10–15 Å), a significant component of the roughness may be due to an incompletely-crosslinked *a*-Si:H layer in contact with the plasma.[32] Such a transition layer is estimated to be ~4–5 Å thick, and its effect may lead to the higher void fraction for the nucleation-induced roughness layer. Changes in the geometry of the roughness and the nature of the transition layer may also account for the gradual increase in f_v during coalescence in Fig. 10 from 0.4 at the onset of bulk layer growth to 0.5 at $d_b = 100$ Å.

We also comment on the extent to which microstructural analysis by SE is model dependent. Such a claim can be made because the extraction of the microstructural parameters and optical properties relies on the assumption of an effective medium model of uncertain validity. In the analysis of SE data to obtain the sample structure and optical properties simultaneously, it is often difficult to overcome the correlations that prevent one from identifying the correct EMT formulation, particularly with a limited data set. The present study, however, has shown that several important film growth features of scientific and technological interest are essentially independent of the chosen EMT. First, the general features of the substrate-induced surface roughness decays in Fig. 4 are not dependent on the selected EMT. Second, the qualitative nucleation and coalescence sequence exhibited by d_s in Fig. 7 is the same for all EMT's. Third, and more importantly, the magnitude of the smoothening effect during coalescence that provides insights into the electronic quality of the resulting *a*-Si:H film[45,46] lies within a range of ± 1 Å for all EMT's. Lastly, the bulk layer deposition rate in Fig. 7 is also independent of the EMT formulation. As a result, we conclude that the real-time SE features related to material quality assessment and device design are not significantly model dependent.

Finally, the present study has shown that when the one- and two-layer models for film nucleation and growth are used along with the EMA to simulate the dielectric functions of the nucleating and roughness layers, χ remains near unity and shows no significant increases with time. This demonstrates that the experimental spectra and the best fits to these spectra differ by no more than the random and systematic experimental errors. As a result, it is not fruitful to consider more sophisticated multiparameter EMT's since a simple one-parameter version is sufficient to explain the full real time SE data sets and yield an excellent linear correlation with AFM. Reassessments of the one-parameter EMT's may be warranted in the future as instrumentation for real-time SE improves to yield higher precision or accuracy, or a wider spectral range.[52]

V. SUMMARY

In numerous spectroscopic ellipsometry (SE) studies of semiconductor and metallic materials and thin films, the single-parameter Brugggeman effective medium approximation (EMA) has been used in data analysis for the characterization of sample properties.[17] This reliance on the EMA stems from work by Aspnes *et al.* performed two decades ago in which rough amorphous silicon thin film surfaces were characterized by SE.[15] Since this original work, further assessments of the suitability of the different effective medium theories have been rare. In the present study, we have exploited the more recent advances in real time SE instrumentation to revisit this problem with much larger data sets, collected during the evolution of inhomogeneous layers. We have considered three types of hydrogenated amorphous silicon (*a*-Si:H) layers: (i) two opaque layers (>2500 Å thick) on microcrystalline SnO_2:F and Si:H with substrate-induced roughness ranging from 40 to 80 Å in thickness, (ii) a very thin layer (5–200 Å) on a *c*-Si substrate with nucleation-induced roughness ranging from 10 to 20 Å in thickness, and (iii) a nucleating layer on a Cr substrate described by clusters 5 to 20 Å in thickness. One- and two-layer optical models were used for the *a*-Si:H films in which case the nucleating or surface roughness layers were simulated as single layers consisting of mixtures of *a*-Si:H and void. Five different one-parameter EMT's were employed to calculate the dielectric functions of these mixtures from component material dielectric functions and their volume fractions.

In all cases, the prior result of Ref. 15 has been reaffirmed, namely the EMA was found to provide the best description for all sets of data, consisting of as few as 8 and as many as 200 pairs of (ψ, Δ) spectra (2.48 to 4.00 eV) collected during materials preparation. For the surface roughness on opaque *a*-Si:H, the $q = 1$ limit and LL EMT formulations provided unacceptable results whereas the data could be acceptably described by the EMA, MG, and the $q = 0$ limit formulations. For the nucleation and growth of *a*-Si:H on *c*-Si and Cr, the EMA was much more strongly favored over the other formulations. Measures of surface roughness by atomic force microscopy and by SE analysis with the EMA yield an excellent linear correlation over the range from ~5 to 100 Å in the SE-deduced roughness layer thicknesses. This result provides support for the validity of the general SE-modeling approach in which surface roughness is treated as a discrete layer with effective optical properties, and the lack of such a correlation for two of the five EMT formulations (LL and $q = 1$) provide further support for ruling these out. A final important result of this paper is the observation that many of the quantitative features used to characterize the nucleation, coalescence, and growth of

a-Si:H on smooth substrates for assessment of material suitability for devices are virtually insensitive to the choice of the EMT from the $q=0$ to 1 limits. This result demonstrates that the key information deduced from the SE measurements is model-independent.

ACKNOWLEDGMENTS

This research was supported by the National Science Foundation under Grant Nos. DMR-9622774 and DMR-9820170.

*Present address: Electrotechnical Laboratory, Thin Film Silicon Solar Cells SuperLaboratory, Tsukuba-shi, Ibaraki 305-8568, Japan.

[1] J. M. Bennett and L. Mattsson, *Introduction to Surface Roughness and Scattering* (Optical Society of America, New York, 1990), Vol. 1.
[2] P. Beckmann and A. Spizzichino, *The Scattering of Electromagnetic Waves from Rough Surfaces* (Pergamon, Oxford, 1963).
[3] I. Ohlidal and F. Lukes, Opt. Acta **19**, 817 (1972).
[4] A. A. Maradudin and D. L. Mills, Phys. Rev. B **11**, 1392 (1975).
[5] E. Kretschmann and E. Kroger, J. Opt. Soc. Am. **65**, 150 (1975).
[6] W. L. Mochan and R. G. Barrera, Phys. Rev. B **32**, 4984 (1985).
[7] D. E. Aspnes, Thin Solid Films **89**, 249 (1982).
[8] G. A. Niklasson, C. G. Granqvist, and O. Hunderi, Appl. Opt. **20**, 26 (1981).
[9] O. Hunderi, Surf. Sci. **96**, 1 (1980).
[10] D. V. Sivukhin, Zh. Eksp. Teor. Fiz. **30**, 374 (1956) [Sov. Phys. JETP **3**, 269 (1956)].
[11] R. M. A. Azzam and N. M. Bashara, *Ellipsometry and Polarized Light* (North-Holland, Amsterdam, 1977).
[12] G. E. Jellison, Jr., Thin Solid Films **234**, 416 (1993).
[13] C. A. Fenstermaker and F. L. McCrackin, Surf. Sci. **16**, 85 (1969).
[14] D. E. Aspnes, in *Optical Properties of Solids: New Developments*, edited by B. O. Seraphin (North-Holland, Amsterdam, 1976), Chap. 15, p. 799.
[15] D. E. Aspnes, J. B. Theeten, and F. Hottier, Phys. Rev. B **20**, 3292 (1979).
[16] D. E. Aspnes, E. Kinsbron, and D. D. Bacon, Phys. Rev. B **21**, 3290 (1980).
[17] R. W. Collins, D. E. Aspnes, and E. A. Irene, Spectroscopic Ellipsometry; Proc. 2nd Int. Conference on Spectroscopic Ellipsometry (Elsevier, Amsterdam, 1998).
[18] F. K. Urban, III, P. Ruzakowski Athey, and M. S. Islam, Thin Solid Films **253**, 326 (1994).
[19] J. Koh, Y. Lu, C. R. Wronski, Y. Kuang, R. W. Collins, T. T. Tsong, and Y. E. Strausser, Appl. Phys. Lett. **68**, 1297 (1996).
[20] J. C. Maxwell-Garnett, Philos. Trans. R. Soc. London, Ser. A **203**, 385 (1904).
[21] J. C. Maxwell-Garnett, Philos. Trans. R. Soc. London, Ser. A **205**, 237 (1906).
[22] S. Norrman, T. Andersson, C. G. Granqvist, and O. Hunderi, Phys. Rev. B **18**, 674 (1978).
[23] F. Hottier and J. B. Theeten, J. Cryst. Growth **48**, 644 (1980).
[24] Y. Z. Hu, D. J. Diehl, Q. Liu, C. Y. Zhao, and E. A. Irene, Appl. Phys. Lett. **66**, 700 (1995).
[25] Y. Z. Hu, D. J. Diehl, C. Y. Zhao, C. L. Wang, Q. Liu, E. A. Irene, K. N. Christensen, D. Venable, and D. M. Mayer, J. Vac. Sci. Technol. B **14**, 744 (1995).
[26] R. W. Collins, Rev. Sci. Instrum. **61**, 2029 (1990).
[27] H. V. Nguyen, I. An, and R. W. Collins, Phys. Rev. B **47**, 3947 (1993).
[28] H. V. Nguyen, Y. Lu, S. Kim, M. Wakagi, and R. W. Collins, Phys. Rev. Lett. **74**, 3880 (1995).
[29] D. E. Aspnes, A. A. Studna, and E. Kinsbron, Phys. Rev. B **29**, 768 (1984).
[30] P. N. Sen, C. Scala, and M. H. Cohen, Geophysics **46**, 781 (1981).
[31] D. S. McLachlan, J. Phys. C **19**, 1339 (1986).
[32] R. Robertson and A. Gallagher, J. Appl. Phys. **59**, 3402 (1986).
[33] H. V. Nguyen, I. An, R. W. Collins, Y. Lu, M. Wakagi, and C. R. Wronski, Appl. Phys. Lett. **65**, 3335 (1994).
[34] I. An, Y. Cong, N. V. Nguyen, B. S. Pudliner, and R. W. Collins, Thin Solid Films **206**, 300 (1991).
[35] N. V. Nguyen, B. S. Pudliner, I. An, and R. W. Collins, J. Opt. Soc. Am. A **8**, 919 (1991).
[36] H. Fujiwara, J. Koh, C. R. Wronski, and R. W. Collins, Appl. Phys. Lett. **74**, 3687 (1999).
[37] Y. Z. Hu, J. Joseph, and E. A. Irene, J. Vac. Sci. Technol. A **11**, 1786 (1993).
[38] Y. Cong, I. An, K. Vedam, and R. W. Collins, Appl. Opt. **30**, 2692 (1991).
[39] I. An, Y. M. Li, C. R. Wronski, H. V. Nguyen, and R. W. Collins, Appl. Phys. Lett. **59**, 2543 (1991).
[40] I. An, H. V. Nguyen, A. R. Heyd, and R. W. Collins, Rev. Sci. Instrum. **65**, 3489 (1994).
[41] P. I. Rovira, A. S. Ferlauto, I. An, H. Fujiwara, J. Koh, R. J. Koval, C. R. Wronski, and R. W. Collins, Mater. Res. Soc. Symp. Proc. **557**, 719 (1999).
[42] R. W. Collins and B. Y. Yang, J. Vac. Sci. Technol. B **7**, 1155 (1989).
[43] A. Mazor, D. J. Srolovitz, P. S. Hagan, and B. G. Bukiet, Phys. Rev. Lett. **60**, 424 (1988).
[44] G. E. Jellison, Jr., Appl. Opt. **30**, 3354 (1991).
[45] Y. M. Li, I. An, H. V. Nguyen, C. R. Wronski, and R. W. Collins, Phys. Rev. Lett. **68**, 2814 (1992).
[46] J. Koh, Y. Lee, H. Fujiwara, C. R. Wronski, and R. W. Collins, Appl. Phys. Lett. **73**, 1526 (1998).
[47] G. E. Jellison, Jr., and F. Modine, Appl. Phys. Lett. **69**, 371 (1996); **69**, 2137 (1996).
[48] L. Ley, in *The Physics of Hydrogenated Amorphous Silicon II*, edited by J. D. Joannopoulos and G. Lucovsky (Springer, Berlin, 1984), Vol. 56, p. 61.
[49] Y. Toyoshima, K. Arai, A. Matsuda, and K. Tanaka, Appl. Phys. Lett. **56**, 1540 (1990).
[50] N. Blayo and B. Drevillon, J. Non-Cryst. Solids **137–138**, 771 (1991).
[51] H. Fujiwara, Y. Toyoshima, M. Kondo, and A. Matsuda, Phys. Rev. B **60**, 13 598 (1999).
[52] J. A. Zapien, R. W. Collins, and R. Messier, Mater. Res. Soc. Symp. Proc. **569**, 71 (1999).